$M1$ bands and intruder bands in ^{113}In

R. S. Chakrawarthy and R. G. Pillay
Tata Institute of Fundamental Research, Bombay 400 005, India
(Received 11 January 1996; revised manuscript received 3 September 1996)

High spin states in ^{113}In have been established up to 6.2 MeV in excitation energy and to a tentative spin of $(43/2^-)$ through the reaction ^{110}Pd(^{7}Li, $4n$)^{113}In at a beam energy of 40 MeV. In-beam measurements involved γ-γ coincidences, angular distribution of emitted gamma rays, and directional correlation of oriented states. $M1$ bands consisting of $\Delta I=1$ dipole transitions have been observed. Possible quasiparticle configurations suggest that these bands are similar to the shears bands observed in Pb nuclei. Two intruder bands based on the $\pi h_{11/2}$ orbital and $\pi g_{7/2}$ orbital have been observed. Results of the total Routhian surface and cranked shell model calculations are compared with the experimental data. Alignment features of the intruder bands in the $N=62$ and 64 isotones are discussed. [S0556-2813(97)06201-8]

PACS number(s): 21.10.Re, 27.60.+j, 23.20.En, 23.20.Lv

I. INTRODUCTION

Nuclei bordering the $Z=50$ shell closure have been known to exhibit rotational bands coexisting with single particle states [1–4]. The occurrence of deformed states is due to particle-hole (p-h) excitations of the $Z=50$ Sn core to the deformation driving orbitals that intrude from above the shell gap. The low excitation energy of the intruder states is a consequence of the attractive proton-neutron force that results in a large binding energy gain for such configurations relative to the normal ones [5,6]. Recent experiments in this mass region have resulted in a wealth of data for the collective bands that extend to very high spins, in particular, intruder bands involving proton p-h excitation have been observed in several isotopes of Sn [7–10], Sb [11–15], and ^{111}In [16]. More recently, such intruder bands have also been found in ^{113}I, ^{112,114}Te [17–19] nuclei involving 4p-2h excitations of the Sn core. Interesting features of very low dynamic moment of inertia were observed at high rotational frequencies in the spectra of these nuclei. This feature was interpreted as a smooth termination of a collective rotational band [20,21].

In the case of the In nuclei, it is expected that the excitation of the odd proton occupying the upsloping $g_{9/2}$ orbital to the steeply downsloping deformed orbitals will lead to a deformed state. The essential difference between the rotational bands in In and Sn nuclei is, in Sn nuclei the bands involve π2p-2h excitation, whereas, in In nuclei it is π1p-2h excitation, thus leading to a smaller quadrupole moment. Such an effect has been observed in the study of ^{111}In by Mullins *et al.* [16], where the $\pi h_{11/2}$ band was found to have a smaller deformation value, $\beta_2=0.18$, compared to the ^{113}Sb $\pi h_{11/2}$ band that was deduced to have a deformation value of $\beta_2=0.32$ [13].

Extensive experimental and theoretical studies have been done to understand the properties of low-lying levels in In isotopes [22–31]. The low energy excitations of odd-mass In isotopes cannot be described as being due to pure single hole character or single hole states coupled to the 2^+ quadrupole vibrational state in the Sn isotopes. Experimental evidence exists for the presence of collective phenomena in these levels [3,23,32]. In ^{115,117}In Backlin *et al.* [23] and in ^{117}In Pandharipande *et al.* [32] have suggested that the low spin positive parity states are members of a band built on the $K=1/2^+$ [431] Nilsson state. Extensive experimental and theoretical studies by Heyde *et al.* [3] were done in several In isotopes. They have developed a unified theory to understand the properties of low-lying states in these isotopes that were not understood within the hole-core coupling model. The calculations were specifically done to understand the structure of the positive parity rotational states and the coexisting vibrational states. The rotational states are due to the 1p-2h excitations across the $Z=50$ proton closed shell. Total potential energy calculations of In isotopes by Heyde *et al.* [33] predict a oblate deformed minimum at $\beta_2=-0.18$ associated with the $11/2^-$ [505] orbital, while calculations by Dietrich *et al.* [34] predict a prolate minimum at $\beta_2=0.2$ due to the $1/2^+$ [431] orbital for ^{113}In. The intruder bandhead excitation energy has an A dependence and is lowest at the mid-shell region $N=66$, when the neutron shell is half filled. It is expected that the intruder bandhead in ^{113}In should be at a lower excitation energy compared to the lighter isotopes of In.

The motivation of the present experiment was to search for collective structures in ^{113}In for which very little high-spin data exists. In the previous study of ^{113}In by Tuttle *et al.* [35,36] the low-lying levels up to $I^\pi=(23/2^-)$ and $I^\pi=(17/2^+)$ have been observed. In this work, we report the observation of two intruder rotational bands and bands consisting of magnetic dipole transitions. The rotational bands are interpreted to be based on the $\pi h_{11/2}$ and $\pi g_{7/2}$ orbitals. The dipole bands have similarities with the recently observed ''shears'' bands in singly closed shell nuclei [37]. Qualitative arguments are given for the structure of these bands. Configuration-dependent crossing frequency has been observed in the intruder rotational bands and is discussed within the total Routhian surface and cranked shell-model calculations.

II. EXPERIMENTAL DETAILS

High spin states in ^{113}In were populated using the reaction ^{110}Pd(^{7}Li, 4n)^{113}In, at the 14 UD TIFR-BARC Pelletron

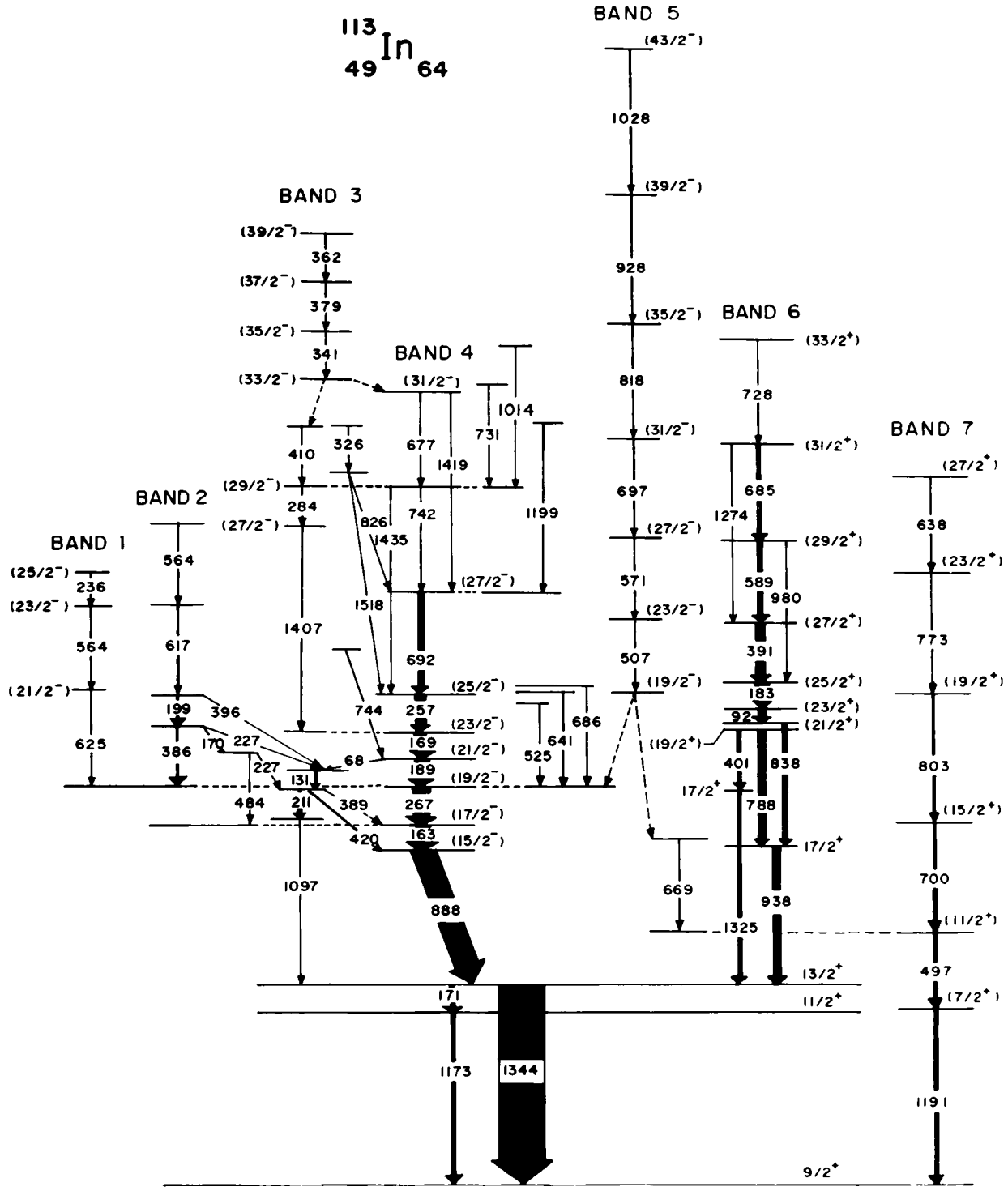

FIG. 1. The level scheme of ^{113}In from the present experiment. Transition energies are marked in keV. The discrete transitions connecting band 3 and band 5 to the low-lying states have not been observed—only the feeding into those states has been indicated by dashed lines.

accelerator in Bombay, India. This reaction was chosen because of its large cross section for the production of ^{113}In between beam energies of 35 to 45 MeV, with relatively little competition from other channels. The target consisted of a 4 mg/cm^2 ^{110}Pd (enrichment 98%) rolled onto a 120 mg/cm^2 Pb backing, thick enough to stop the recoiling nuclei. The enriched ^{110}Pd powder was first annealed in a hydrogen furnace and was subsequently electron-beam melted to remove absorbed moisture and other gases. The purified Pd pellet was rolled to the desired thickness. Gamma rays emitted in this reaction were detected using five Compton-suppressed high-purity germanium detectors (CS-HPGe), used in conjunction with an eight element NaI multiplicity filter. In the γ-γ coincidence experiment the five CS-HPGe

TABLE I. Gamma rays assigned to ^{113}In.

E_γ(keV) [a]	$I_\gamma^{(rel)}$ [b]	Initial state → Final state [c]	A_2/A_0	A_4/A_0	R_{dco} [d]	R_{dco} [e]	Multi-polarity [f]
68.6	17(2)	2.851→2.783					
91.8	122(2)	$(23/2^+)\rightarrow(21/2^+)$	-0.24(1)	0.02(2)	0.9(3)	0.57(5)	$(M1/E2)$
131.8	33(1)	2.783→2.652					
163.2	443(4)	$(17/2^-)\rightarrow(15/2^-)$	-0.32(1)	0.07(2)	0.9(3)	0.49(1)	$(M1/E2)$
169.5	254(2)	$(23/2^-)\rightarrow(21/2^-)$	-0.28(1)	0.07(3)	0.86(3)	0.45(4)	$(M1/E2)$
170.2 [g]	44(3)	3.049→2.879					
171.5		$13/2^+\rightarrow11/2^+$			0.9(3)	0.57(5)	$M1/E2$
183.3	194(1)	$(25/2^+)\rightarrow(23/2^+)$	-0.34(1)	0.08(3)	0.9(3)	0.55(3)	$(M1/E2)$
189.7	228(2)	$(21/2^-)\rightarrow(19/2^-)$	-0.29(1)	0.01(3)	0.81(8)	0.58(4)	$(M1/E2)$
199.1	39(1)	3.247→3.048					
211.7	17(2)	2.652→2.441					
226.7 [g]	23(2)	3.048→2.821					
		2.879→2.652					
236.1	17(2)	$(25/2^-)\rightarrow(23/2^-)$			1.26(22)		$(M1/E2)$
256.9	167(2)	$(25/2^-)\rightarrow(23/2^-)$	-0.27(4)	0.01(3)	1.0(4)	0.59(5)	$(M1/E2)$
267.5	349(2)	$(19/2^-)\rightarrow(17/2^-)$	-0.24(1)	0.02(2)	1.04(3)	0.57(5)	$(M1/E2)$
271.1 [h]	12(2)						
278.2 [h]	56(1)						
284.5	12(2)	$(29/2^-)\rightarrow(27/2^-)$			0.87(22)		$(M1/E2)$
326.2	<10	5.121→4.795					
340.8	25(2)	$(35/2^-)\rightarrow(33/2^-)$			0.86(19)		$(M1/E2)$
362.1	16(2)	$(39/2^-)\rightarrow(37/2^-)$			1.05(10)		$(M1/E2)$
377.2 [h]							
379.1	15(2)	$(37/2^-)\rightarrow(35/2^-)$			1.15(36)		$(M1/E2)$
386.5	45(2)	3.048→2.662			0.95(7)	0.55(10)	$(M1/E2)$
388.9	63(2)	$2.652\rightarrow(17/2^-)$			1.18(11)	0.47(12)	$(M1/E2)$
390.9	167(3)	$(27/2^+)\rightarrow(25/2^+)$	-0.15(1)	0.08(1)	1.13(14)	0.52(5)	$(M1/E2)$
395.8	19(1)	3.247→2.851			1.06(18)	0.53(10)	$(M1/E2)$
401.8	70(2)	$(19/2^+)\rightarrow17/2^+$	-0.22(3)	0.08(4)		0.61(20)	$M1/E2$
409.7 [g]	24(2)	$5.121\rightarrow(29/2^-)$			0.9(3)		$(M1/E2)$
420.4	42(3)	$2.652\rightarrow(15/2^-)$			0.94(17)	0.49(15)	$(M1/E2)$
474.3 [h]	10(2)						
483.9	23(2)	2.879→2.395			0.84(22)		
497.3	90(3)	$(11/2^+)\rightarrow(7/2^+)$	0.20(2)	-0.08(4)		0.9(1)	$E2$
507.1	25(2)	$(23/2^-)\rightarrow(19/2^-)$	0.27(4)	0.01(3)		0.9(3)	$E2$
525.9	35(2)	$3.187\rightarrow(19/2^-)$			0.97(12)		
564.8 [g]	23(2)	$(23/2^-)\rightarrow(21/2^-)$			1.2(3)		$(M1/E2)$
		4.428→3.864					
571.8	63(2)	$(27/2^-)\rightarrow(23/2^-)$	0.21(4)	-0.02(3)		0.9(3)	$E2$
589.4	72(2)	$(29/2^+)\rightarrow(27/2^+)$	-0.29(2)	0.02(1)	0.9(3)	0.49(2)	$(M1/E2)$
617.2	45(3)	3.864→3.247			1.11(16)		
625.3	28(2)	$(21/2^-)\rightarrow(19/2^-)$			1.1(3)		$(M1/E2)$
637.8	31(2)	$(27/2^+)\rightarrow(23/2^+)$					$(E2)$
641.1	15(2)	$3.303\rightarrow(19/2^-)$					
677.7	17(2)	$(31/2^-)\rightarrow(29/2^-)$			1.08(30)		$(M1/E2)$
684.6	47(2)	$(31/2^+)\rightarrow(29/2^+)$	-0.27(4)	0.01(3)		0.48(16)	$(M1/E2)$
686.1	<10	$3.348\rightarrow(19/2^-)$					
692.6	68(2)	$(27/2^-)\rightarrow(25/2^-)$			1.08(13)	0.57(17)	$(M1/E2)$
697.1	12(2)	$(31/2^-)\rightarrow(27/2^-)$				0.9(2)	$E2$
700.4	85(2)	$(15/2^+)\rightarrow(11/2^+)$				0.9(2)	$E2$
728.2	31(2)	$(33/2^+)\rightarrow(31/2^+)$	-0.23(3)	0.05(2)			$(M1/E2)$
731.6	<10	$5.442\rightarrow(29/2^-)$					
742.4	25(2)	$(29/2^-)\rightarrow(27/2^-)$			0.89(23)		$(M1/E2)$
744.6	19(2)	$3.595\rightarrow(21/2^-)$					

TABLE I. (*Continued*).

E_γ(keV) [a]	$I_\gamma^{(rel)}$ [b]	Initial state → Final state [c]	A_2/A_0	A_4/A_0	R_{dco} [d]	R_{dco} [e]	Multipolarity [f]
772.9	51(3)	$(23/2^+)\rightarrow(19/2^+)$	0.23(2)	-0.06(2)			$E2$
788.2	124(2)	$(19/2^+)\rightarrow 17/2^+$	-0.24(1)	0.02(2)		0.68(2)	$(M1/E2)$
803.2	80(2)	$(19/2^+)\rightarrow(15/2^+)$	0.18(2)	-0.06(2)		0.9(2)	$E2$
818.2	23(4)	$(35/2^-)\rightarrow(31/2^-)$				1.1(3)	$E2$
826.3	<10	$4.795\rightarrow(27/2^-)$					
838.9	87(2)	$(21/2^+)\rightarrow 17/2^+$	0.20(2)	-0.10(4)		0.95(8)	$E2$
888.7	515(3)	$(15/2^-)\rightarrow(13/2^-)$	-0.275(6)	0.012(3)	0.80(3)	0.44(2)	(E1)
919.2 [h]	31(3)						
928.4	<20	$(39/2^-)\rightarrow(35/2^-)$					$(E2)$
938.7	256(2)	$17/2^+\rightarrow 13/2^+$	0.297(8)	-0.072(6)		0.99(4)	$E2$
980.2	<10	$(29/2^+)\rightarrow(25/2^+)$					$(E2)$
991.5 [h]	56(1)						
1014.6	33(3)	$5.725\rightarrow(29/2^-)$					
1028.3(6)	<20	$(43/2^-)\rightarrow(39/2^-)$					$(E2)$
1097.9	24(2)	$2.441\rightarrow 13/2^+$					
1173.2	25(2)	$11/2^+\rightarrow 9/2^+$			1.41(35)		$M1/E2$
1191.3	88(3)	$(7/2^+)\rightarrow(9/2^+)$					$(M1/E2)$
1274.2	<5	$(31/2^+)\rightarrow(27/2^+)$					$(E2)$
1324.6	82(2)	$17/2^+\rightarrow 13/2^+$	0.26(4)	-0.05(2)		0.89(9)	$E2$
1344.5	1000	$13/2^+\rightarrow 9/2^+$	0.260(4)	-0.045(2)	1.77(8)	1.07(6)	$E2$
1390.3 [h]	<10						
1406.7	14(2)	$(27/2^-)\rightarrow(23/2^-)$			1.9(5)		$E2$
1418.6	14(3)	$(31/2^-)\rightarrow(27/2^-)$					$(E2)$
1434.9	32(3)	$(29/2^-)\rightarrow(25/2^-)$	0.16(4)	-0.15(6)	1.7(5)		$E2$
1444.5 [h]	<10						
1518.3	14(3)	$4.795\rightarrow(25/2^-)$					
1583.5 [h]	14(3)						

[a]The errors are given on the last digit. Transition energies accurate to within ± 0.3 keV, unless otherwise quoted.
[b]Intensities are normalized to 1000 for the 1344 keV γ transition.
[c]For γ transitions having no spin-parity assignments, the initial and final excitation energies are given in MeV.
[d]The gating transition(s) is a dipole.
[e]The gating transition(s) is a quadrupole.
[f]Multipolarity for known transitions adopted from previous works.
[g]Intensity quoted for doublet.
[h]Transition identified as belonging to ^{113}In, but not placed in the level scheme.

detectors were at angles 15°, ±45°, and ±75° to the beam axis. The individual counting rates in each of the CS-HPGe detectors were less than 10 kHz at a beam current of 1.5 p nA. The excitation function was done between beam energies of 35 and 45 MeV, and the relative cross section of ^{113}In was found to peak at 40 MeV in agreement with the statistical model code CASCADE.

The γ-γ coincidence data was collected at a beam energy of 40 MeV comprised of twofold Ge events, detected within a time window of 400 ns and qualified by a hardware trigger of multiplicity greater than one in the NaI detectors. A total of 40×10^6 coincidence events were accumulated. The energy and efficiency calibrations of the CS-HPGe detectors were done using radioactive sources of ^{133}Ba and ^{152}Eu. The γ-γ coincidence data from the five CS-HPGe detectors were sorted off-line by gain matching each of the detectors using the ^{152}Eu and ^{133}Ba data. The background-corrected projected spectra generated with gates on the gamma transitions were used to construct the level scheme.

The angular distribution of the gamma rays were measured with the five CS-HPGe detectors at angles 15°, 30°, 44°, 60°, and 90° with respect to the beam axis. These were analyzed by fitting the efficiency-corrected intensities to the distribution function of Legendre polynomial

$$W(\theta)=A_0+A_2P_2(\cos\theta)+A_4P_4(\cos\theta). \quad (1)$$

The relative efficiency of the detectors was obtained by collecting the radioactive data during the experiment. The ratio of directional correlation of oriented states (R_{dco}) of the γ transitions was constructed by the following procedure:

$$R_{dco}=\frac{(I_{\gamma1}@15^\circ \text{ gated by } \gamma_2@75^\circ)}{(I_{\gamma1}@75^\circ \text{ gated by } \gamma_2@15^\circ)}, \quad (2)$$

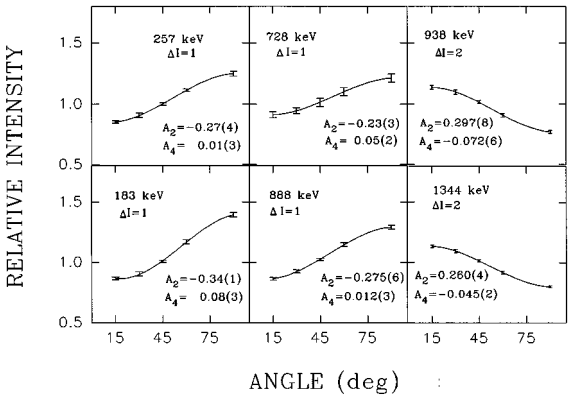

FIG. 2. Angular distribution plots of few γ transitions in ^{113}In.

where the gating transition γ_2, has either a pure dipole or quadrupole multipolarity. When gated by a quadrupole transition the $R_{\rm dco}$ value was close to 1.0 for stretched $E2$ transitions and close to 0.5 for stretched dipole transitions. Similarly, with a dipole gating transition, the $R_{\rm dco}$ values was close to 2 and 1 for quadrupole and dipole transitions, respectively. The $R_{\rm dco}$ ratios were calibrated using known transitions. The $R_{\rm dco}$ values for band 4 were obtained using the sum gate of 163 and 267 keV γ transitions and for weak γ transitions the sum gate of 163, 267, and 256 keV γ transitions was used. The $R_{\rm dco}$ value for band 6 was obtained using the sum gate of 1344 and 938 keV γ transitions, which are of $E2$ multipolarity. Similarly, γ transitions deduced to be of $E2$ multipolarity from the angular distribution data were used as gating transitions to obtain the $R_{\rm dco}$ values in band 7. The multipolarity of γ transitions, which were contaminated in the singles angular distribution data could be extracted from the $R_{\rm dco}$ values. The spin assignments have been made assuming that the high spin states subsequently decay to levels with a lower spin.

III. EXPERIMENTAL RESULTS

The level scheme deduced from the present experiment is shown in Fig. 1. Table I contains the details of γ-transition energies, relative intensities, A_2 and A_4 values, spin assignments, and the $R_{\rm dco}$ values. The γ-ray intensities have been obtained from the total projection of the list mode data with full time window and for overlapping γ transitions the intensities were obtained from the 1344 keV gate and normalized. Low energy transitions with the assumed multipolarity gave the correct intensity balance, since in this mass region the $M1$ and $E1$ conversion coefficients differ considerably.

The two dominant cascades in the decay of ^{113}In are built on the previously known 888 and 938 keV γ transitions. Angular distribution data assigns a dipolar character to the 888 keV γ transition deexciting from the negative parity level at $I^{\pi}=(15/2^{-})$. Parity assignment is based on comparison with neighboring nuclei (where negative parity states are excited with more intensity) and is tentative. Figure 2 shows angular distribution plots of few γ transitions in ^{113}In. The level scheme is ordered numerically from band 1 to band 7. The discussion of each of the bands is given in the following subsections.

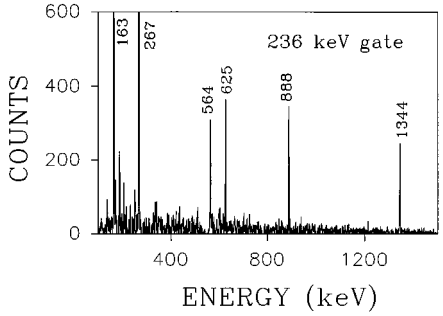

FIG. 3. Gated spectrum with the gate set on the 236 keV γ transition.

A. Band 1

A relatively weak set of γ transitions, viz. the 236, 564, and 625 keV feed the $I^{\pi}=(19/2^{-})$ energy level. The $R_{\rm dco}$ values for these γ transitions when gated by dipole transitions is close to unity, hence they have been assigned $M1/E2$ multipolarity. This band extends to a tentative spin of $(25/2)\hbar$. Approximately 2.7(3)% of the total intensity is carried by this band. Figure 3 shows the 236 keV gated spectrum.

B. Band 2

The coincident γ transitions 564, 617, 199, and 386 keV are members of this band. Several γ transitions depopulate states in this band and feed the energy levels of band 4 at $I^{\pi}=(17/2^{-})$ and $I^{\pi}=(19/2^{-})$. The gated spectra do not show any coincidences with the members of band 1, so a second 564 keV γ transition is placed in this band.

C. Band 3

The set of coincident γ transitions 341, 379, and 362 keV decay into states of band 4. The $R_{\rm dco}$ values support their assignment as dipole transitions. From this data set no crossover $E2$ transitions were observed in this band. Figure 4 shows the projected spectrum with the gate set on the 341 keV γ transition. Two decay paths of this band were identified, but it was difficult to place the exact excitation energy of this band. The spin-parity assignment for this band is tentative.

D. Band 4

The previously known series of intense dipole transitions comprised of 163, 267, 189, and 169 keV γ transitions has been extended in spin from $I^{\pi}=(23/2^{-})$ to $I^{\pi}=(31/2^{-})$. A representative spectrum for these transitions is shown in Fig. 5, which shows the spectrum gated by the 257 keV γ transition. The multipolarity of the band members has been deduced from both the angular distribution and $R_{\rm dco}$ data. Most of the population of ^{113}In comes through this band. The $I^{\pi}=(25/2^{-})$ state in this band is fed by a sequence comprising of 692, 742, and 677 keV γ transitions. The observation of high-energy $E2$ crossover transitions (1435 and 1419 keV) has helped to extract the $B(M1;I\rightarrow I\text{-}1)/B(E2;I\rightarrow I\text{-}2)$ ratio (see Table II). Since the transition probability is proportional to E_{γ}^{2I+1} the high-energy intraband

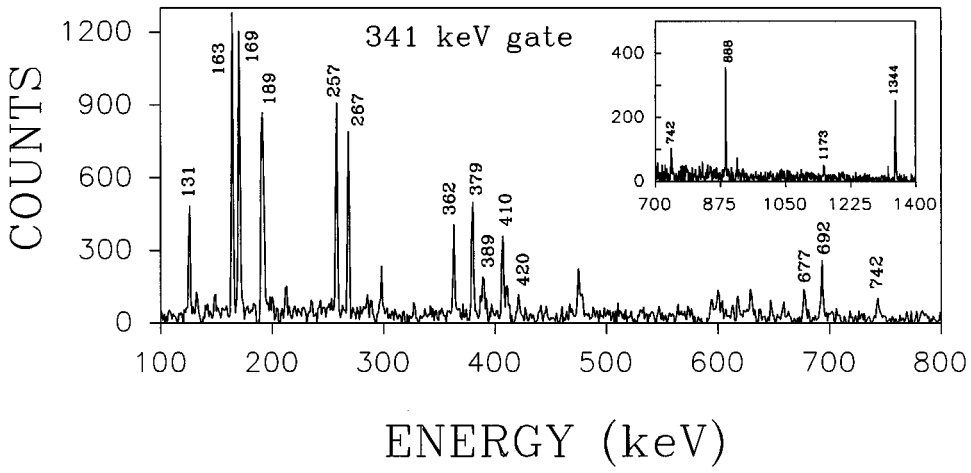

FIG. 4. Gated spectrum with the gate set on the 341 keV γ transition. The inset depicts high-energy γ transitions.

quadrupole transitions compete with that of lower energy dipole transitions and therefore the crossover $E2$ transitions are more probable at the top of the band (similar features exist in band 6). The presence of crossover $E2$ transitions also pins down the magnetic character of the dipole transitions (this argument assumes that there is no octupole deformation in this mass region).

Several γ transitions feed into levels of band 4. The previously known cascade comprised of the 1097, 211, and 131 keV γ transitions [36] has been confirmed in the present work. Based on the intensities from the coincidence data we infer the presence of second 170 and 227 keV γ transitions. The 484 keV γ transition is in coincidence with the low-lying energy levels and differs from the earlier placements reported in Ref. [36]. The 420 and 389 keV γ transitions depopulate from states of this cascade and feed the $I^{\pi}=(15/2^{-})$ and $I^{\pi}=(17/2^{-})$ energy levels of band 4. Also, the 525, 641, and 686 keV γ transitions feed the $I^{\pi}=(19/2^{-})$ state, and the 744 keV γ transition feeds the $I^{\pi}=(21/2^{-})$ state. While, the 326, 826, and 1518 keV γ transitions feed the $I^{\pi}=(27/2^{-})$ and $I^{\pi}=(25/2^{-})$ levels, differing from the placements of the earlier work [36]. Figure 6 shows the spectrum gated by the 1518 keV γ transition. Furthermore, the 1199 keV γ transition feeds into the $I^{\pi}=(27/2^{-})$ state and the 731 and 1014 keV γ transitions feed the $I^{\pi}=(29/2^{-})$ state. The multiple branches make the coincidence spectra complex, but also provide consistency checks on the level scheme. On this basis, many of the γ transitions have been, unambiguously, placed in the level scheme.

E. Band 5

The analysis of the data has revealed a coincident sequence comprising of 507, 571, 697, 818, 928, and 1028 keV γ transitions, which are members of this rotational band. Figure 7 displays the sum of the background subtracted coincidence spectra gated by all the band members. This band has a relative intensity of less than 4%. The angular distribution of the 507 and 571 keV γ transitions is indicative of $E2$ multipolarity. Using the sum gate of these two γ transitions the $R_{\rm dco}$ values of 697 and 818 keV γ transitions were found to be close to unity. It has not been possible to extract the multipolarity of the higher-lying γ transitions in this band due their weak intensity or of contamination in the angular distribution data. The 377, 409, and 669 keV γ transitions are involved in the decay of this band but firm links to the low-lying levels could not be established. In addition,

TABLE II. Branching ratios in the $M1$ bands.

$M1$ (keV)	$E2$ (keV)	$B(M1)/B(E2)(\mu_N^2/e^2b^2)$
677	1419	17(6)
742	1435	8(2)
685	1274	71(14)
589	980	24(6)

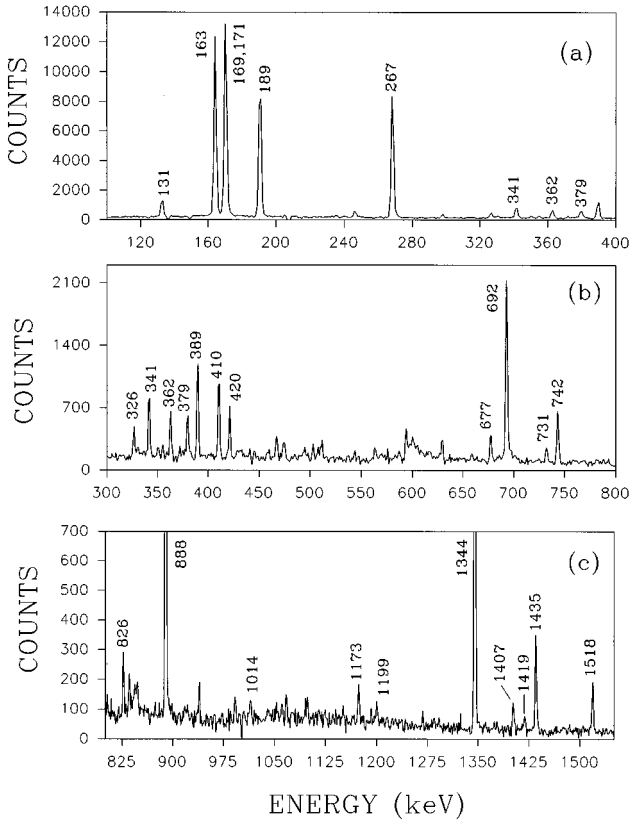

FIG. 5. The three panels, viz. (a), (b), and (c) depict the spectra gated by the 257 keV γ transition.

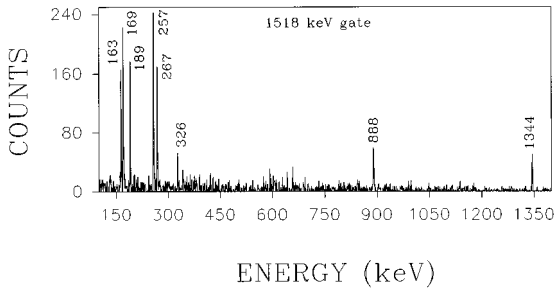

FIG. 6. Gated spectrum with the gate set on the 1518 keV γ transition.

this band feeds into band 7 via the 669 keV γ transition. The spin of the decay-out state of this band has been tentatively assigned to be $(19/2^-)$.

F. Band 6

The set of γ transitions consisting of 92, 183, 391, 589, 685, 728, 980, and 1274 keV constitute band 6. Figure 8 shows the spectrum gated by the 589 keV γ transition. From the angular distribution of the 938 and 838 keV γ transitions a positive A_2 value was deduced. Thus, these γ transitions were inferred to be of $E2$ multipolarity. For intensity balance the 92 keV γ was deduced to be a $M1/E2$ transition, hence for the remaining members of this band a positive parity has been assigned. This positive parity rotational-like dipole band decays through the 788, 838, and 401 keV γ transitions. Coincidence conditions among 838 and 788 keV gates require an unobserved 50 keV γ transition. The angular distribution of 183, 391, and 589 keV γ transitions indicate their dipole ($M1/E2$) nature. In addition, weak crossover γ-transitions, viz. 980 and 1274 keV, have been observed. The deduced experimental $B(M1)/B(E2)$ ratio is presented in Table II, using the formula,

$$\frac{B(M1)}{B(E2)} = 0.6968 \frac{E_\gamma^5(I \to I-2)}{\lambda E_\gamma^3(I \to I-1)} (\mu_N^2/e^2b^2),$$

where

$$\lambda = \frac{T_\gamma(I \to I-2)}{T_\gamma(I \to I-1)},$$

is the γ-ray branching ratio between the $\Delta I=2$ and $\Delta I=1$ transitions in a band. This assumes that the $\Delta I=1$ transitions are pure $M1$ transitions (i.e., mixing ratio $\delta=0$).

G. Band 7

The set of γ transitions 497, 700, 603, 773, and 638 keV constitute members of band 7. Figure 9 depicts the spectrum gated by the 497 keV γ transition. The previous study due to [36] has identified the 1191 keV γ transition depopulating the $I^\pi = 7/2^+$ state. This state was identified by them to belong to the Nilsson state originating from the π [413]1/2$^+$ orbital. The tentatively placed 497 and 700 keV γ transitions have been confirmed in this experiment and, in addition, this band has been extended in spin from $I^\pi=(15/2^+)$ to $(27/2^+)$. The spin assignments for this band are based on the angular distribution and $R_{\rm dco}$ data.

IV. DISCUSSION

A. Total Routhian surface and cranked shell model calculations

The total Routhian surface calculation (TRS) based on Woods-Saxon potential using monopole pairing interaction was performed [38]. Figure 10 shows results of this calculation at various frequencies in the rotating frame of the nucleus. The universal set of parameters employed in the calculations are described in Ref. [39]. For the positive parity configurations, at low frequencies a noncollective prolate minima is predicted at $\beta_2=0.09$ and $\gamma=-120°$ [Fig. 10(a)]. This is consistent with the low-lying levels, which are vibrational in nature. At $\hbar\omega=0.495$ MeV a prolate shape with $\beta_2=0.116$ and $\gamma=-2°$ is yrast [Fig. 10(b)]. For the negative parity configurations involving a proton in the $h_{11/2}$ orbital, a prolate deformed minima with $\beta_2=0.191$ and $\gamma=5.0°$ is ap-

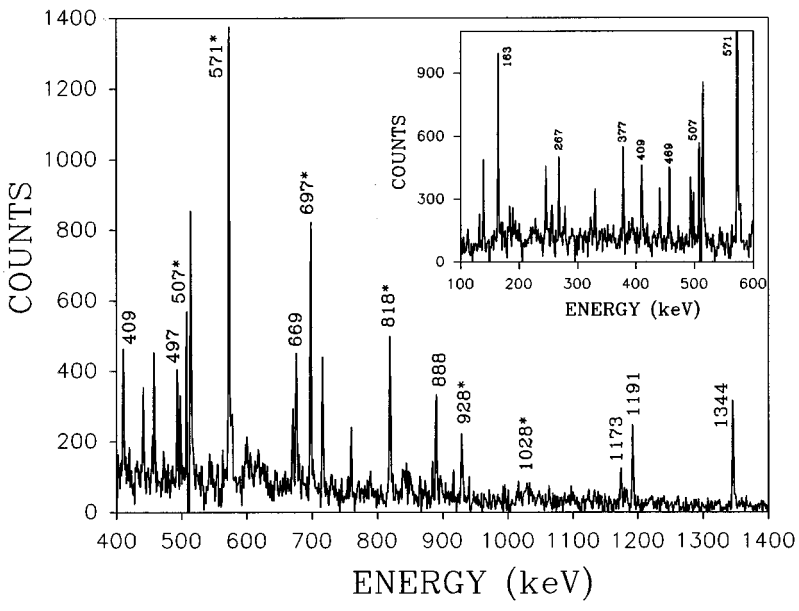

FIG. 7. Sum of γ-ray spectra gated by the members of the $\pi h_{11/2}$ intruder band. Gating transitions have been marked as an asterisk. The inset depicts γ transitions up to 600 keV. The other unlabeled γ transitions are the contaminant γ rays due to the overlap of some of the gating transitions with γ decays from other nuclei.

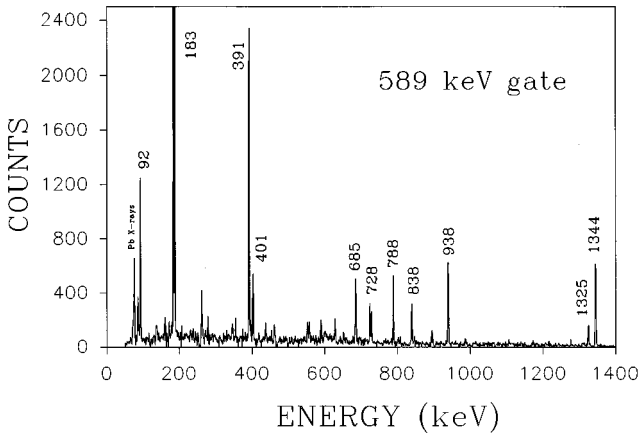

FIG. 8. Gated spectrum with the gate set on the 589 keV γ transition.

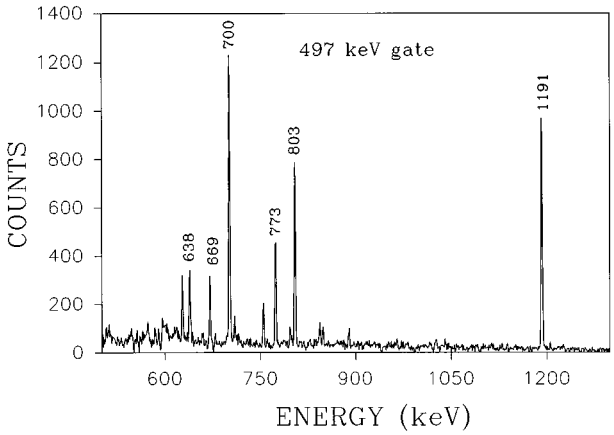

FIG. 9. Gated spectrum with the gate set on the 497 keV γ transition.

parent at $\hbar\omega=0.495$ MeV [Fig. 10(c)]. The cranked shell-model calculations with the TRS calculated deformation value predict the first alignment due to a pair of $h_{11/2}$ neutrons at $\hbar\omega=0.40$ MeV. The calculated neutron Routhians are shown in Fig. 11.

B. Low-lying levels

Nuclei near closed shells are near spherical in their ground state. In these nuclei the high angular momentum states are built by aligning the individual particle angular momenta along the symmetry axis and the resulting level schemes are characterized by irregular level spacings. The ground-state spin parity of ^{113}In is $9/2^+$, due to the odd proton in the $g_{9/2}$ subshell. The branching ratio of the 171 keV $M1/E2$ to the 1344 keV $E2$ transition is 0.04(1), which was obtained from the 938 keV gate. Tuttle *et al.* [35] have reported a value of 0.02(1) from their Coulomb excitation measurement. Similarities exist between the low-lying states of Sn nuclei, which are near spherical or vibrational, and the In nuclei. The low-lying states in the ^{105,107,109,111,113}In isotopes, viz. the $11/2^+$ and $13/2^+$ [40] states have been interpreted as due to the coupling of $g_{9/2}$ proton hole to the adjacent Sn's 2^+ vibrational state [30,31]. However, this model does not take into account quasiparticle excitations, which is needed to account for the high spin states.

C. Dipole bands: Band 4 and band 6

The dominant feature present in band 4 and band 6 is the sequence of transitions that do not extend to high spins and are characterized by large $B(M1)/B(E2)$ ratios. These two facts indicate that the intrinsic structure of band 4 and band 6 is not that of a well-deformed nucleus. It is to be mentioned here that in the $A\sim200$ mass region, rotational-like sequences of levels have been observed that are connected by unusually strong $M1$ transitions [$B(M1)\sim1$–$10\ \mu_N^2$] having almost no $E2$ strength [$B(E2)\sim$ 10 W.u.]. The tilted axis cranking calculations suggest that in these bands the spins of the valence protons align along the symmetry axis, while the spins of the valence neutrons align along the axis of rotation. With increasing spin, these two components tilt towards each other, while the direction of the total spin remains unchanged [37]. Such structures are expected to appear in the Sn region and more generally in nuclei near closed shells [41], due to the interaction of high-j particle and hole configurations of protons and neutrons. More importantly, even the presence of a deformed field is not necessary for its appearance.

In ^{113}In, for states above 3 MeV it is expected that quasiparticle excitations become important. The lowest band crossing in this mass region is due to alignment of $h_{11/2}$ neutrons. Potential energy surface calculations predict a small prolate deformation ($\beta_2=0.09$) for this configuration [42]. At such low deformations, the neutrons occupy the low-Ω states of the $h_{11/2}$ orbital. A shear mechanism is one possibility to account for the positive parity states. Hence, band 6 may possibly involve a configuration of aligned $h_{11/2}$ neutrons in low-Ω orbitals coupled to a $\pi g_{9/2}$ hole. In such a coupling scheme, the high-j particle and hole angular momentum vectors are approximately perpendicular at the bandhead. This allows one to estimate the bandhead spin empirically, which for this configuration is $19/2^+$ (assuming that aligned neutrons contribute $10\hbar$). In the level scheme the band begins at a spin value of $(21/2^+)$, supporting this approximate geometry. We rule out proton excitations across the $Z=50$ shell gap for these states, as this will lead to occupation of the deformation driving orbitals and manifest in a rotational band of $E2$ transitions. Alternatively, configurations giving rise to the same spin value would involve a fully aligned ($\pi g_{9/2}^{-1}\nu d_{5/2}\nu g_{7/2}$) configuration, for which no band would be observed. In ^{111}In, a similar positive parity structure has been recently identified, beginning at $I^\pi = 21/2^+$ [43]. In the same nucleus a second $21/2^+$ state is also known due to the fully aligned ($\pi g_{9/2}^{-1}\nu d_{5/2}\nu g_{7/2}$) configuration [44]. The configuration of this state is supported by g-factor measurement [45]. As expected no bands are observed on this isomeric level. In ^{113}In this second $21/2^+$ has not been identified.

An upper limit on the spin can be obtained for the prolate ($g_{9/2}^{-1}\otimes h_{11/2}^2$) configuration in the shears mode. The closing of the two spin vectors generates the angular momentum and this would result in a maximal spin of $29/2^+$ for this configuration. The additional units in spin observed in this band can be due to collective rotation. In the tilted axis coupling scheme [37], the $M1$ transition probability becomes appreciable due to the combination of a small prolate deformation, a significant K value for this configuration and $g_{9/2}$ proton

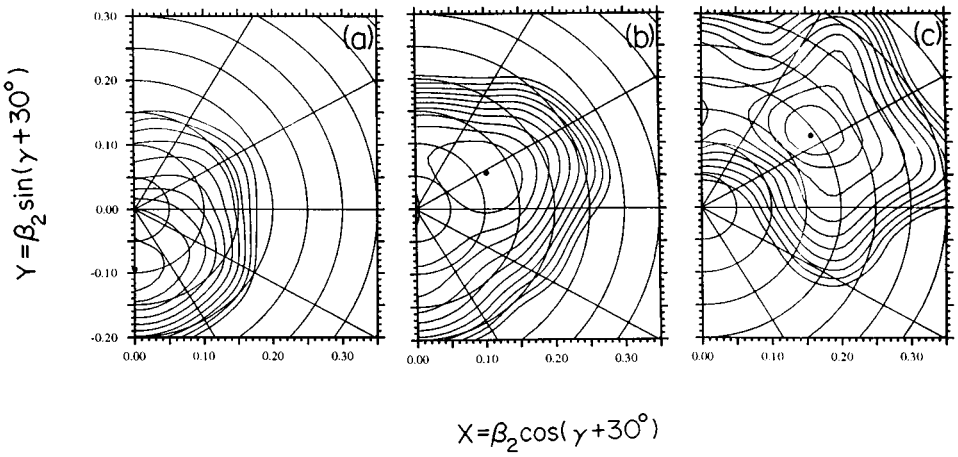

FIG. 10. Total Routhian surface calculations for the configurations $(\pi,\alpha)=(+,1/2)$ at (a) $\hbar\omega=0.062$, and (b) 0.495 MeV, and (c) the $(\pi,\alpha)=(-,-1/2)$ $\pi h_{11/2}$ deformed minima becomes yrast at $\hbar\omega=0.495$ MeV.

hole and thus account for the predominant dipole transitions observed in this band. High-$K(K=8)$ $\Delta I=1$ prolate bands have been observed in the ^{108,109,110}Cd [46–48] isotopes involving the high-K proton holes in $g_{9/2}$ orbital coupled to neutrons in the low-Ω states of the $h_{11/2}$ orbital. The bands in Cd isotopes are inferred to be due to four and six quasiparticle configurations, occurring at higher excitation energies than the ones in ^{111,113}In.

The negative parity states of band 4 do not show a regular band structure and they can be generated with an odd number of neutrons in the $h_{11/2}$ orbital, having a possible configuration of $\nu(g_{7/2})^{-1}(h_{11/2})^{1}\pi(g_{9/2})^{-1}$. The fully aligned configuration will give rise to a spin value of $27/2^-$, in the experimental spectrum there is a break after $25/2^-$ with the transitions of higher energy feeding the compressed spectrum, it is possible that the remaining angular momentum is generated due to some collectivity.

D. Intruder bands: Band 5 and band 7

The alignment plot of band 5 and band 7 is shown in Fig. 12. Band 5 starts at $i_x\sim 5.7\ \hbar$ and the aligned spin increases gradually over the frequency range 0.3–0.5 MeV. The gain in alignment is about $3\hbar$. The gain in alignment for band 7 in the observed frequency range is about $6\hbar$. It is proposed that band 5 is a rotational band due to the $\pi h_{11/2}$ orbital. This is based on comparison of the dynamic moment of inertia ($\mathcal{J}^{(2)}$) of the $\pi h_{11/2}$ intruder band in ^{115}Sb [14] and ^{113}In (Fig. 13), as was done in the case of ^{111}In by Mullins *et al.* [16]. The single proton in $h_{11/2}$ orbital has an i_x approximately $5\hbar$ and the three quasiparticle configuration should have an aligned spin of about $14\hbar$. Since in the present data set the gain in alignment is only about $3\hbar$, which is far below the expected value for a fully aligned configuration, it is obvious that the alignment is gradual. This behavior is in complete contrast to the $\pi h_{11/2}$ band in ^{111}In, which has an aligned spin of about $9\hbar$ [16] at similar frequency. The gradual alignment in band 5 can be due to a large interaction strength between the ground band and the aligned band. This results in the alignment being spread over several frequencies. In odd proton nuclei, in this mass region, the $\nu h_{11/2}$ alignment occurs at much higher frequency and with a large interaction strength when compared to similar crossing in the core Sn nucleus [12]. The $\nu h_{11/2}$ crossing in the core Sn nucleus (^{114}Sn) occurs at $\sim$0.4 MeV; in contrast, the same crossing is not complete even at the highest observed (greater than 0.5 MeV) frequencies in the $\pi h_{11/2}$ bands of the $N=64$ odd proton ^{113}In and ^{115}Sb nuclei. The $\nu h_{11/2}$ crossing frequency is correctly reproduced using the spin projected Hartree-Bogoliubov calculations for the even-even ^{110,112,114}Sn nuclei [8], whereas it is underpredicted for the odd proton nuclei by the present cranking calculations using the universal set of parameters. Such shifts in crossing frequencies have been inferred by Janzen *et al.* in the ^{113}Sb $\pi h_{11/2}$ band as signatures of residual n-p interaction between the $h_{11/2}$ proton and the aligning $h_{11/2}$ neutrons [13].

In the previous study [36] two γ transitions of band 7 were identified to be members of the $\pi g_{7/2}$ intruder rotational band. The present study extends this band to higher spins. Interestingly, in contrast to band 5, the alignment plot of band 7 shows a sharp upbend at $\hbar\omega\sim 0.39$ MeV. The observed upbend is attributed to the alignment of $h_{11/2}$ neutrons, being the lowest band crossing in this mass region. The crossing frequency and gain in alignment is, as expected, close to the one observed in the 2p-2h band of ^{114}Sn. The sharp upbend implies a weak interaction between the aligned and the nonaligned structures. Unlike the $\pi h_{11/2}$ orbital, the $\pi g_{7/2}$ orbital has lesser spatial overlap with the $h_{11/2}$ neutrons, which possibly accounts for the observed sharp alignment feature in this band.

E. Comparison of the intruder bands with the neighboring nuclei

It is instructive to compare the alignment features of the intruder bands in the neighboring nuclei. In Table III, the known $\nu h_{11/2}$ crossing frequencies of the bands in Sn, In, and Sb nuclei are presented. The intruder band data for $N=66$ is scarce and for $N<60$ the observed bands do not extend to low frequencies and are thought to be built on aligned neutrons [7,8,11]. Figure 13 depicts the dynamic moment of inertia ($\mathcal{J}^{(2)}$), as a function of rotational frequency, for intruder bands in the $N=62$ and 64 isotopes. The intruder bands in ^{112,114}Sn nuclei display sharp crossings, whereas in the ^{113,115}Sb and ^{111,113}In isotopes this feature is gradual and the crossings are shifted to higher frequencies than in the corresponding core Sn nuclei [12,14] (Table III). Within the framework of the cranked shell model, the crossings can be shifted to higher frequencies due to a variety of effects, such as changes in deformation, pairing, and higher multipole mo-

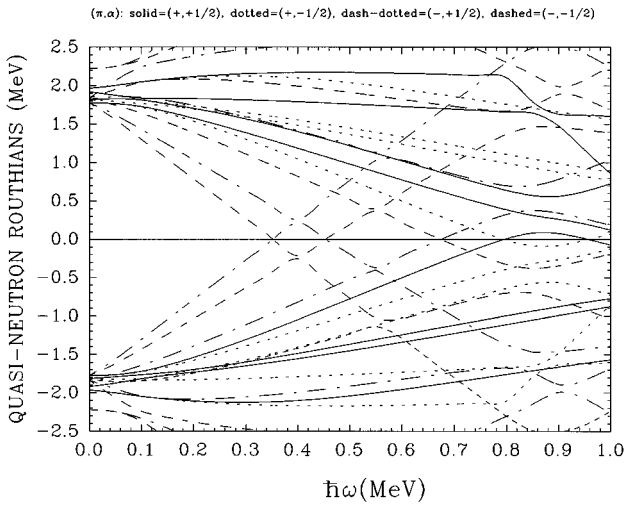

FIG. 11. The neutron Routhians calculated according to the cranked shell model.

ments like β_4. If one compares the $\mathcal{J}^{(2)}$ plots of ^{111,113}In, which have the same deformations but different behavior in their alignments [Fig. 13(b)], also ^{111}In and ^{113}Sb, which have been experimentally shown to have different deformations but similar alignment behavior [16], then clearly the first alignment in these nuclei, which is always due to the $\nu h_{11/2}$ is independent of changes in deformation. It is to be noted here that the total Routhian surface calculation predicts correctly the deformation in ^{111}In, and the value predicted for ^{113}In is not very much different. Changes in the other parameters will not result in such large shifts in the crossing frequencies [13]. In general, cranked shell-model calculations do not fully take into account the residual interactions and hence do not seem to reproduce the alignment behavior for intruder bands in odd proton (neutron) nuclei correctly. Recent calculations by Satula *et al.* [49] involving explicitly the quadrupole-quadrupole *n-p* interaction could account partially for the shifts in the crossing frequencies, although, as pointed out by them, large shifts in crossing frequencies of about 0.1 MeV and gradual alignment are difficult to account

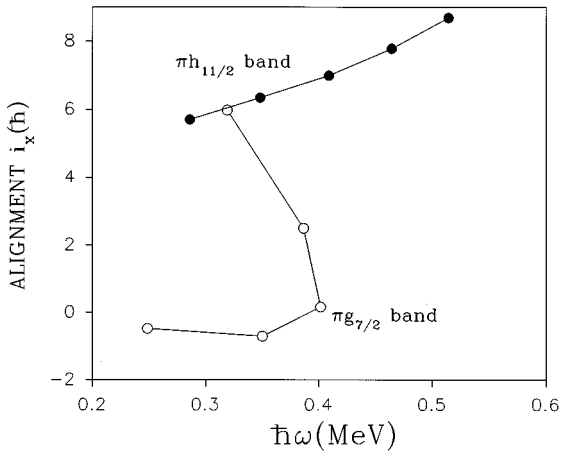

FIG. 12. Alignment plot of the $\pi h_{11/2}$ intruder band (band 5) and $\pi g_{7/2}$ intruder band (band 7). The reference parameter was $\mathcal{J}_0 = 22\hbar^2$/MeV, similar to the ^{111}In value in Ref. [16].

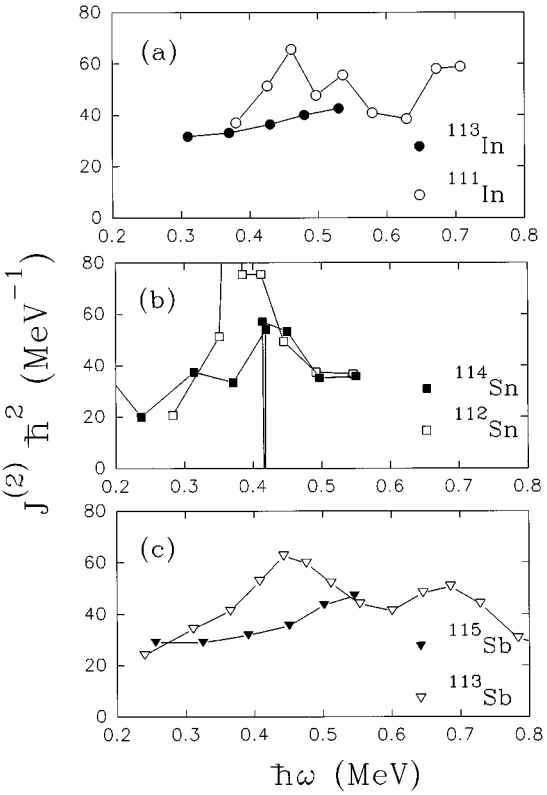

FIG. 13. The dynamic moment of inertia plots ($\mathcal{J}^{(2)}$) of the intruder bands in the $N=62$ and $N=64$ isotones.

for. Schematic single-*j* shell cranking calculations including the *n-p* interaction also predict shifts in the crossing frequencies for the mass-80 and mass-110 nuclei when protons and neutrons simultaneously occupy the $g_{9/2}$ and $h_{11/2}$ subshells, respectively [50,51].

V. SUMMARY AND CONCLUSIONS

High spin states have been investigated in ^{113}In. Bands consisting of predominantly magnetic dipole transitions and two rotational bands due to the $\pi g_{7/2}$ and $\pi h_{11/2}$ orbitals have been observed. In the $\pi h_{11/2}$-based band the first neutron alignment is delayed with respect to ^{114}Sn within the framework of cranked shell-model calculations. In this mass region, this delay is a feature of the odd proton nuclei, when the odd proton and the aligning neutrons are occupying the same $h_{11/2}$ orbital. In the heavier odd proton nuclei such features have been accounted for due to the quadrupole type of pairing [52]. Wu points out that the anomalous delay of the band crossing in decoupled bands of odd proton nuclei is due to the decoupling term in the particle rotor model [53]. However, in the $A\sim 110$ mass region the reason for the odd

TABLE III. $\nu h_{11/2}$ crossing frequencies for the Sn, In, and Sb nuclei.

Neutrons	Sn $\hbar\omega$(MeV)	In $\hbar\omega$(MeV)	Sb $\hbar\omega$(MeV)
60	<0.38		0.41
62	0.37	0.46	0.46
64	0.41	>0.53	>0.5

proton nuclei showing different alignment behavior than the core even-even nuclei seems to be due to neutron-proton (n-p) type of pairing. It would thus be of interest to probe the effects of n-p correlations on the electromagnetic transition rates and g factors in the backbend region.

Within the tilted axis cranking approach (which takes into account the rotational perturbation effects on the high-K band correctly), angular momentum in high K bands is generated due to collective rotation as well as shearing of the high-j particle and hole angular momenta. The fraction of angular momentum shared between these two modes depends on deformation. The important feature that emerges as one studies the high-K prolate $\pi g_{9/2}^{-1}$ bands, is that this configuration evolves progressively into a well-deformed configuration [reflected in the $B(M1)/B(E2)$ values] in the Sb, I, and Cs [54] nuclei. On the other hand at low deformations, such as in In nuclei, the ''shears'' mechanism dominates to generate angular momentum for such configurations.

ACKNOWLEDGMENTS

We would like to thank the Pelletron accelerator staff for the smooth operation of the machine. We are grateful to S. D. Paul, A. Chatterjee, and B. Srinivasan for their help during the experiment. Useful discussions with Professor C. V. K. Baba and Professor C. R. Praharaj are acknowledged. Dr. Ramon Wyss is thanked for providing the TRS maps. We are grateful to D. C. Ephrahim and the late A. R. Pednekar, of the target laboratory, for their assistance during target preparation. We acknowledge Dr. R. K. Bhowmik of Nuclear Science Center, New Delhi for providing the graphic display software.

[1] J. Bron, W. H. A. Hesselink, A. van Poelgeest, J. J. A. Zalmstra, M. J. Uitzinger, H. Verheul, K. Heyde, M. Waroquier, H. Vincx, and P. Van Isacker, Nucl. Phys. **A318**, 335 (1979).

[2] A. van Poelgeest, J. Bron, W. H. A. Hesselink, K. Allaart, J. J. A. Zalmstra, M. J. Uitzinger, and H. Verheul, Nucl. Phys. **A346**, 70 (1980).

[3] K. Heyde, P. Van Isacker, M. Waroquier, J. L. Wood, and R. A. Meyer, Phys. Rep. **102**, 291 (1983).

[4] J. L. Wood, K. Heyde, W. Nazarewicz, M. Huyse, and P. Van Duppen, Phys. Rep. **215**, 101 (1992).

[5] K. Heyde, P. Van Isacker, R. F. Casten, and J. L. Wood, Phys. Lett. **155B**, 303 (1985).

[6] G. F. Arenas Peris and P. Federman, Phys. Lett. B **173**, 359 (1986).

[7] R. Wadsworth, H. R. Andrews, R. M. Clark, D. B. Fossan, A. Galindo-Uribarri, J. R. Hughes, V. P. Janzen, D. R. LaFosse, S. M. Mullins, E. S. Paul, D. C. Radford, H. Schnare, P. Vaska, D. Ward, J. N. Wilson, and R. Wyss, Nucl. Phys. **A559**, 461 (1993).

[8] H. Harada, T. Murakami, K. Yoshida, J. Kasagi, T. Inamura, and T. Kubo, Phys. Lett. B **207**, 17 (1988); H. Harada, M. Sugawara, H. Kusakari, H. Shinohara, Y. Ono, K. Furuno, T. Hosoda, M. Adachi, S. Matsuki, and N. Kawamura, Phys. Rev. C **39**, 132 (1989).

[9] M. Schimmer, R. Wirowski, S. Albers, G. Bohm, A. Dewald, A. Gelberg, and P. von Brentano, Z. Phys. A **338**, 117 (1991).

[10] M. Schimmer, S. Albers, A. Dewald, A. Gelberg, R. Wirowski, and P. von Brentano, Nucl. Phys. **A539**, 527 (1992).

[11] V. P. Janzen, D. R. LaFosse, H. Schnare, D. B. Fossan, A. Galindo-Uribarri, J. R. Hughes, S. M. Mullins, E. S. Paul, L. Persson, S. Pilotte, D. C. Radford, I. Ragnarsson, P. Vaska, J. C. Waddington, R. Wadsworth, D. Ward, J. Wilson, and R. Wyss, Phys. Rev. Lett. **72**, 1160 (1994).

[12] D. R. LaFosse, D. B. Fossan, J. R. Hughes, Y. Liang, H. Schnare, P. Vaska, M. P. Waring, J.-y. Zhang, R. M. Clark, R. Wadsworth, S. A. Forbes, E. S. Paul, V. P. Janzen, A. Galindo-Uribarri, D. C. Radford, D. Ward, S. M. Mullins, D. Prévost, and G. Zwartz, Phys. Rev. C **50**, 1819 (1994).

[13] V. P. Janzen, H. R. Andrews, B. Haas, D. C. Radford, D. Ward, A. Omar, D. Prévost, M. Sawicki, P. Unrau, J. C. Waddington, T. E. Drake, A. Galindo-Uribarri, and R. Wyss, Phys. Rev. Lett. **70**, 1065 (1993).

[14] R. S. Chakrawarthy and R. G. Pillay, Phys. Rev. C **54**, 2319 (1996); in *Book of Abstracts*, International Nuclear Physics Symposium, Bombay, 1995, (Bhabha Atomic Research Center, Bombay, 1995), p. A-74.

[15] D. R. LaFosse, D. B. Fossan, J. R. Hughes, Y. Liang, P. Vaska, M. P. Waring, and J.-y. Zhang, Phys. Rev. Lett. **69**, 1332 (1992).

[16] S. M. Mullins, V. P. Janzen, P. Vaska, D. B. Fossan, G. Hackman, D. R. LaFosse, E. S. Paul, D. Prévost, H. Schnare, J. C. Waddington, R. Wadsworth, D. Ward, and M. P. Waring, Phys. Lett. B **318**, 592 (1993).

[17] E. S. Paul, C. W. Beausang, S. A. Forbes, S. J. Gale, A. N. James, P. M. Jones, M. J. Joyce, R. M. Clark, K. Hauschild, I. M. Hibbert, R. Wadsworth, R. A. Cunningham, J. Simpson, T. Davinson, R. D. Page, P. J. Sellin, P. J. Woods, D. B. Fossan, D. R. LaFosse, H. Schnare, M. P. Waring, A. Gizon, and J. Gizon, Phys. Rev. C **48**, R490 (1993).

[18] E. S. Paul, C. W. Beausang, S. A. Forbes, S. J. Gale, A. N. James, P. M. Jones, M. J. Joyce, H. R. Andrews, V. P. Janzen, D. C. Radford, D. Ward, R. M. Clark, K. Hauschild, I. M. Hibbert, R. Wadsworth, R. A. Cunningham, J. Simpson, T. Davinson, R. D. Page, P. J. Sellin, P. J. Woods, D. B. Fossan, D. R. LaFosse, H. Schnare, M. P. Waring, A. Gizon, J. Gizon, T. E. Drake, J. DeGraaf, and S. Pilotte, Phys. Rev. C **50**, 698 (1994).

[19] I. Thorslund, D. B. Fossan, D. R. LaFosse, H. Schnare, K. Hauschild, I. M. Hibbert, S. M. Mullins, E. S. Paul, I. Ragnarsson, J. M. Sears, P. Vaska, and R. Wadsworth, Phys. Rev. C **52**, R2839 (1995).

[20] I. Ragnarsson, V. P. Janzen, D. B. Fossan, N. C. Schmeing, and R. Wadsworth, Phys. Rev. Lett. **74**, 3935 (1995).

[21] A. V. Afanasjev and I. Ragnarsson, Nucl. Phys. **A591**, 387 (1995).

[22] C. W. Tang, A. Pakkanen, Z. C. Mester, C. D. Coryell, G. Chilosi, K. Bos, and A. H. Wapstra, Z. Phys. A **272**, 301 (1975).

[23] A. Backlin, B. Fogelberg, and S. G. Malmskog, Nucl. Phys. **A96**, 539 (1967).

[24] H. J. Kim and R. L. Robinson, Phys. Rev. C **9**, 767 (1974).
[25] S. Harar and R. N. Horoshko, Nucl. Phys. **A183**, 161 (1972).
[26] C. V. Weiffenbach and R. Tickle, Phys. Rev. C **3**, 1668 (1971).
[27] J. McDonald, B. Fogelberg, A. Backlin, and Y. Kawase, Nucl. Phys. **A224**, 13 (1974).
[28] R. G. Markham and H. W. Fulbright, Phys. Rev. C **9**, 1633 (1974).
[29] V. Sergeev, J. Becker, L. Eriksson, L. Gidefeldt, and L. Holmberg, Nucl. Phys. **A202**, 385 (1973).
[30] S. Sen, Nucl. Phys. **A191**, 29 (1972).
[31] A. Covello, V. R. Manfredi, and N. Azziz, Nucl. Phys. **A201**, 215 (1973).
[32] V. R. Pandharipande, K. G. Prasad, and R. P. Sharma, Nucl. Phys. **A104**, 525 (1967).
[33] K. Heyde, M. Waroquier, H. Vincx, and P. Van Isacker, Phys. Lett. **64B**, 135 (1976).
[34] W. Dietrich, A. Backlin, C. O. Lannergard, and I. Ragnarsson, Nucl. Phys. **A253**, 429 (1975).
[35] W. K. Tuttle, P. H. Stelson, R. L. Robinson, W. T. Milner, F. K. McGowan, S. Raman, and W. K. Dagenhart, Phys. Rev. C **13**, 1036 (1976).
[36] J. Lyttkens, K. Nilson, and L. P. Ekström, Nucl. Data Sheets **33**, 1 (1981).
[37] G. Baldsiefen, H. Hubel, W. Korten, D. Mehta, N. Nenoff, B. V. Thirumala Rao, P. Willsau, H. Grawe, J. Heese, H. Kluge, K. H. Maier, R. Schubart, S. Frauendorf, and H. J. Maier, Nucl. Phys. **A574**, 521 (1994); S. Frauendorf, Nucl. Phys. **A557**, 259c (1993).
[38] R. Wyss, W. Satula, W. Nazarewicz, and A. Johnson, Nucl. Phys. **A511**, 324 (1990).
[39] W. Nazarewicz, J. Dudek, R. Bengtsson, T. Bengtsson, and I. Ragnarsson, Nucl. Phys. **A435**, 397 (1985).
[40] *Table of Isotopes*, 7th ed., edited by C. M. Lederer and V. S. Shirley (Wiley, New York, 1978).
[41] S. Frauendorf, J. Meng, and J. Reif, in *Proceedings of Conference on Physics from Large γ-ray Detector Arrays*, Berkeley, 1994, Vol. 2, p. 52, LBL-35687.
[42] J. A. Sheikh (private communication).
[43] P. Vaska *et al.* (private communication).
[44] W. H. A. Hesselink, J. Bron, P. M. A. van der Kam, V. Paar, A. van Poelgeest, and A. G. Zephat, Nucl. Phys. **A299**, 60 (1978).
[45] P. van Nes, K. Allaart, W. H. A. Hesselink, Jan Konijn, and H. Verheul, Z. Phys. A **301**, 137 (1981).
[46] I. Thorslund, C. Fahlander, J. Nyberg, S. Juutinen, R. Julin, M. Piiparinen, R. Wyss, A. Lampinen, T. Lönnroth, D. Müller, S. Törmänen, and A. Virtanen, Nucl. Phys. **A564**, 285 (1993).
[47] S. Juutinen, P. Simecek, C. Fahlander, R. Julin, J. Kumpulainen, A. Lampinen, T. Lönnroth, A. Maj, S. Mitarai, D. Müller, J. Nyberg, M. Piiparinen, M. Sugawara, I. Thorslund, S. Törmänen, and A. Virtanen, Nucl. Phys. **A577**, 727 (1994).
[48] S. Juutinen, R. Julin, M. Piiparinen, P. Ahonen, B. Cederwall, C. Fahlander, A. Lampinen, T. Lönnroth, A. Maj, S. Mitarai, D. Müller, J. Nyberg, P. Simecek, M. Sugawara, I. Thorslund, S. Törmänen, A. Virtanen, and R. Wyss, Nucl. Phys. **A573**, 306 (1994).
[49] W. Satula, R. Wyss, and F. Dönau, Nucl. Phys. **A565**, 573 (1993).
[50] J. A. Sheikh, N. Rowley, M. A. Nagarajan, and H. G. Price, Phys. Rev. Lett. **64**, 376 (1990).
[51] S. Frauendorf, in *Proceedings of the Workshop on Gammasphere Physics*, Berkeley, 1995 (World Scientific, Singapore, in press); S. Frauendorf and J. A. Sheikh, Phys. Rev. Lett. (submitted).
[52] Y. Sun, S. Wen, and D. H. Feng, Phys. Rev. Lett. **72**, 3483 (1994).
[53] C. S. Wu, Phys. Rev. C **51**, 1819 (1995).
[54] Nuclear Structure Laboratory progress report 1990–1992, SUNY at Stony Brook.